

## Probing the Morphology and Energy Landscape of Blends of Conjugated Polymers with Sub-10 nm Resolution

Sebastian Westenhoff,<sup>\*,†</sup> Ian A. Howard, and Richard H. Friend

*OE-Group, Cavendish Laboratory, J. J. Thomson Avenue, Cambridge CB30HE, United Kingdom*

(Received 20 December 2007; revised manuscript received 8 April 2008; published 2 July 2008; corrected 7 July 2008)

We have investigated the charge generation dynamics in intimately mixed blends of polyfluorene copolymers optimized for photocurrent generation. Using femtosecond transient absorption spectroscopy, we find that the charge generation time is limited by exciton diffusion to the interface. Combined with the kinetics of exciton energy migration, the data reveal the blend morphology on a length scale of sub-10 nm. Furthermore, we demonstrate that excitons are guided efficiently to the interface, which is consistent with an accumulation of low energy sites at the heterojunction.

DOI: [10.1103/PhysRevLett.101.016102](https://doi.org/10.1103/PhysRevLett.101.016102)

PACS numbers: 81.07.-b

Organic photovoltaic devices are fabricated from partially demixed organic semiconducting materials, such as conjugated polymers or fullerene derivatives [1–4]. In these devices, light is absorbed in one or both of the active components to form tightly bound excitons. If the offsets of the conduction and valence band states at the heterojunction are appropriate (type II), excitons may ionize efficiently. It has been proposed that unbound charge carriers are generated [5]; however, they may be bound by their mutual Coulomb attraction [3], or excitonic effects may lead to even tighter binding [6]. In any case, there is a general requirement that the light is absorbed no further than an exciton diffusion length from the heterojunction, which is typically assumed to be  $\sim 10$  nm. This is a severe restriction for efficient charge collection, where the polymer phases have to be bicontinuous and extend over the whole film thickness.

At present it is not possible to reliably characterize the size of the nanoscale morphologies of plastic solar cells. This is a major obstacle in the design of more efficient solar cells and fundamentally limits the insight into the early stages of the demixing process in polymer blends. Atomic force microscopy (AFM) may be used to identify surface features with a maximum resolution of 10 nm. The bulk morphology of polymer-polymer blends has been mapped with a resolution of 50 nm using x-ray microscopy [7]. In order to break through this resolution barrier, we develop an alternative approach which makes use of the high mobility of singlet excitons in organic thin films [8–11]. By combining the dynamics of exciton energy migration with a real-time observation of charge generation, we map the morphology of binary polymer blends on a length scale from 1 to 12 nm.

We study mixed blends poly(9,9'-dioctylfluorene-*alt*-benzothiadiazole) (F8BT) and poly(9,9'-dioctylfluorene-*co*-bis-*N*, *N'*-(4, butylphenyl)-bis-*N*, *N'*-phenyl-1,4-phenylene-diamine) (PFB) with molecular weights  $M_p = 135$  kg/mol and  $M_p = 150$  kg/mol, respectively. AFM cannot resolve any features for the films that were spin cast from chloroform and we therefore expect a do-

main size of less than 10 nm [12]. Broadband transient optical absorption spectroscopy with  $\sim 100$  fs time resolution was performed as described in Ref. [12].

Figures 1(a) and 1(b) show time-resolved transient optical absorption spectra of pure F8BT and a blend consisting of 50% F8BT and 50% PFB, respectively. Note that we site selectively excite F8BT at 490 nm, so that no excitons are generated in the higher optical gap material PFB ( $\lambda_{\max} = 390$  nm). In pure F8BT we observe a positive differential transmission signal ( $\Delta T/T$ ) at wavelengths shorter than 620 nm due to excitonic stimulated emission. At longer wavelengths a negative signal due to excitonic photoinduced absorption is recorded [12,13]. The transient absorption spectra of the blends show the same features at early times, which then rapidly evolve into a secondary broad and long lived absorption. We attribute the latter band to cations on PFB and anions on F8BT chains [12–15]. Figure 1(c) shows the time evolution of the signal, spectrally averaged from 530 to 600 nm. It is observed that the time for the evolution from the positive “excitonic” to the negative “charge” signal increases with increasing concentration of F8BT, indicating that the charge generation is limited by diffusion of excitons to the heterojunction.

To deconvolute the exciton and charge signals, we develop a kinetic model based on the rate equations  $\frac{d[Ex]}{dt} = -k_N(t)[Ex] - k_{CT}(t)[Ex]$  and  $\frac{d[CT]}{dt} = k_{CT}(t)[Ex]$  for the time derivatives of the exciton and charge concentration, respectively. The exciton decay rate to the ground state  $k_N(t)$  is time dependent due to exciton-exciton annihilation [13]. The charge generation rate  $k_{CT}(t)$  is limited by exciton diffusion to the heterojunction, which is an intrinsically nonexponential process [11]. In the integrated rate equations we represent these time dependencies as multi-exponential functions  $Ex_{CT}(t) = \sum_{j=1}^4 A_{CT,j} \exp(-k_{CT,j}t)$  and  $Ex_N(t) = \sum_{i=1}^2 A_{N,i} \exp(-k_{N,i}t)$  so that  $[Ex] = Ex_N(t)Ex_{CT}(t)$  and  $[CT] = 1 - Ex_{CT}(t)$ . We fit the kinetics in Fig. 1(c) globally as  $\Delta T/T = N([Ex] + r\tilde{k}_{CT}/(\tilde{k}_{CT} + \tilde{k}_N)[CT])$ , with  $N$  as the number of excitations,  $\tilde{k} = \sum_m A_m k_m$ , and  $r$  as the ratio of the spectrally averaged cross

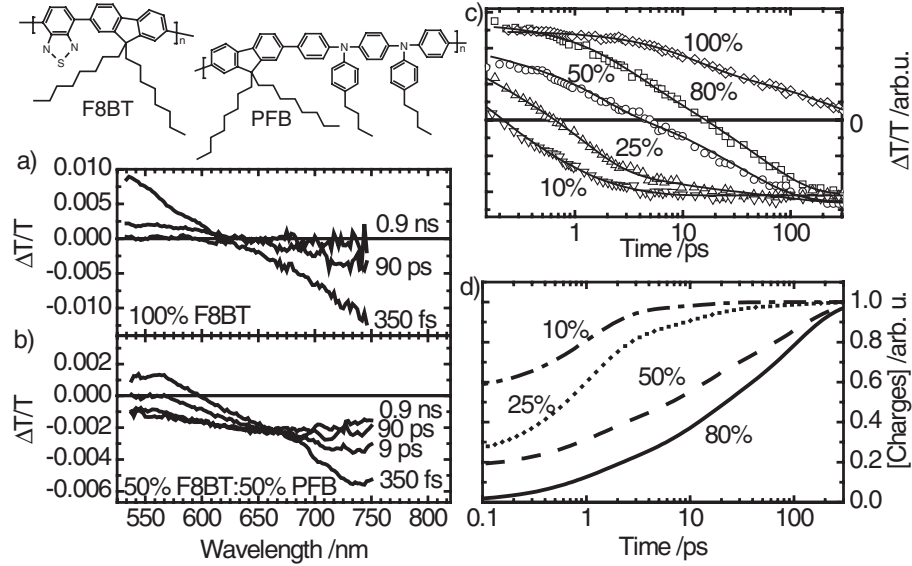


FIG. 1. Panels (a) and (b) show differential transmission spectra of F8BT and a 50%:50% F8BT:PFB blend, respectively, at delay times as indicated in the figure. The markers in panel (c) show the kinetics spectrally integrated from 530 to 600 nm. The F8BT content is indicated and was controlled by manipulating the ratio of F8BT and PFB in solution. The traces are normalized to the number of absorbed photons. The excitation photon flux was  $<1 \times 10^{14}$  photons/cm<sup>2</sup> for all samples and low enough to avoid charge generation by multiphoton interaction [13]. The lines are a global fit as discussed in the text. Panel (d) shows the concentration of charges reconstructed from the fits.

sections of the charge transfer absorption and the stimulated emission.  $\sum_m A_m = 1$  was required during fitting and  $Ex_N(t)$  was determined from the kinetics of the pure F8BT and held constant when fitting the blends [16].

In the best fit, the largest charge generation rate,  $k_{CT,1} = 9.17 \text{ ps}^{-1}$ , is an order of magnitude faster than the characteristic exciton energy transfer rate (see below) and similar to the inverse of the time resolution of the spectroscope (100 fs). We therefore interpret this to be due to excitons that are created at the heterojunction and undergo charge generation during the excitation pulse [17]. Figure 1(d) plots the charge concentration generated from excitons which are created in the bulk ( $2 \leq j \leq 4$ ). It is clearly seen that for increasing concentrations of F8BT the charge generation time increases. This is because exciton diffusion to the interface takes longer when the size of F8BT domains increases. The amplitude at 0.1 ps corresponds to the fraction of charges that are generated from excitons, which are created directly at the heterojunction. The fraction increases with decreasing F8BT concentration. This is because as the domain size decreases, the ratio of interface to bulk sites increases. Thus, the data contain information about the size of the domains in which the excitons migrate. We now seek to determine this by accounting for the time dependence of the exciton diffusion length.

To determine the exciton diffusion length, we have measured and modeled exciton diffusion in F8BT films. In Fig. 2 the energy relaxation of the peak of the stimulated emission of a F8BT film is plotted. This excitonic Stokes shift is caused by exciton energy transfer [11]. To simulate

the random walk of excitons, the film is represented by a cubic grid and the site energy ( $E_i$ ) are randomly assigned from a Gaussian density of states with width  $\sigma_{inh} = 0.06 \text{ eV}$  [10]. In the Monte Carlo simulation the microscopic energy transfer rates are calculated as

$$k_{i \rightarrow j} = \begin{cases} k_{ET} \exp(-(E_j - E_i)/k_B T) & \text{for } E_j - E_i > 0 \\ k_{ET} & \text{for } E_j - E_i \leq 0 \end{cases} \quad (1)$$

with  $k_{ET}$  as the characteristic exciton hopping rate, and  $k_B$  and  $T = 300 \text{ K}$  as the Boltzmann constant and the temperature, respectively. A range from  $k_{ET} = 1/4 \text{ ps}^{-1}$  to  $k_{ET} = 1/2 \text{ ps}^{-1}$  reproduces the experimental Stokes shift well [18]. The root-mean-square (rms) exciton diffusion length ( $R_{max}$ ) is shown in Fig. 2. Assuming an average chromophore length of  $l_{seg} = 3$  monomeric units, a rms exciton displacement of 16 nm is yielded at the lifetime of F8BT (1.6 ns), which is a reasonable value for disordered conjugated polymers.

To determine the domain size from the charge generation time [see Fig. 1(d)] and the exciton diffusion length (see Fig. 2) we first plot the former as a function of the latter to yield the cumulative distribution function of exciton diffusion length prior to charge generation [see Fig. 3(a)]. By computing  $d[\text{Charges}]/dR_{max}$ , the probability density function of the exciton diffusion length prior to charge generation is obtained. These data, shown in Fig. 3(b) for F8BT:PFB blends, are a direct measure of the size of F8BT domains within the blends. It can be seen that the domain size increases with increasing con-

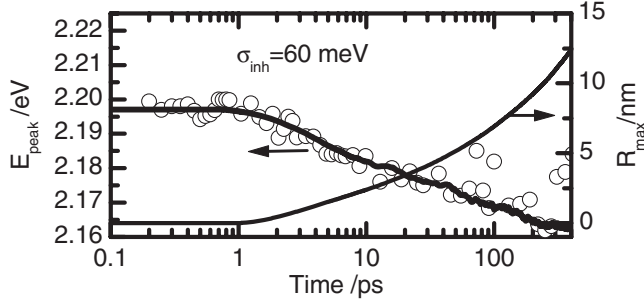


FIG. 2. The symbols show the redshift of the stimulated emission of a film of F8BT. The data were obtained by fitting two Gaussians representing the excitonic photoinduced absorption and stimulated emission to each time-resolved spectrum. Here the center energy of the latter Gaussian is plotted. The line is the simulated average energy of excitons (see text). The right-hand axis is the rms exciton diffusion length, defined here as  $R_{\max}(t) = \sqrt{\langle \max(s(t') \leq t)^2 \rangle}$ , with  $s(t)$  as the displacement of each exciton from its origin, and the brackets  $\langle \rangle$  denoting an ensemble average. Taking the maximum of  $s$  reflects that the excitons will not back-transfer once they arrive at the heterojunction. The distance between grid points was calculated as  $l_{gs} = [(M_{\text{F8BT}} l_{\text{seg}}) / (N_{\text{Av}} \rho_{\text{F8BT}})]^{1/3}$ , with  $\rho_{\text{F8BT}} \approx 1 \text{ g/cm}^3$  for the density of the films,  $M_{\text{F8BT}} = 945 \text{ g/mol}$  as the molecular weight of a F8BT monomer,  $N_{\text{Av}}$  as Avogadro's number, and  $l_{\text{seg}}$  as the number of monomers in a chromophore. For  $l_{\text{seg}} = 3$ , which is a typical value for conjugated polymers [9,22],  $l_{gs} = 1.68 \text{ nm}$  is yielded.

tent of F8BT. The largest domains of the blend containing 10% F8BT have a characteristic length of only  $\sim 2 \text{ nm}$ , whereas for the blend containing 50% F8BT diffusion lengths as large as  $\sim 12 \text{ nm}$  are detected, indicating much larger F8BT domains. For 80% F8BT content the weight of the distribution is shifted to higher diffusion length, which is consistent with an inverted morphology. We have found that the error in the  $x$  direction introduced by the choice of  $k_{ET}$  and  $l_{\text{seg}}$  in the energy transfer model is  $\sim 2 \text{ nm}$  for large distances and significantly smaller for decreasing  $x$  values [16]. The same analysis for blends containing F8BT and poly(9,9-dioctylfluorene-*co*-N-(4-butylphenyl)diphenylamine) (TFB) showed qualitatively the same behavior [16].

In Fig. 3(b) we also show the distribution of exciton diffusion length expected for a sphere with radius  $R = 5 \text{ nm}$  (dashed line) and  $R = 2 \text{ nm}$  (solid line). The theoretical probability density was calculated as the distribution of distances of all sites within the sphere from a point at the interface. It can be seen that while the blend with 25% F8BT concentration overlaps well with the theoretical curve for  $R = 2 \text{ nm}$  (except for small distances  $< 2 \text{ nm}$ , see below), a single spherical phase does not approximate the measurements for the blend containing 50% F8BT well. This indicates that either a distribution of domain sizes is present or that a different morphology, such as bicontinuous phases, is dominant.

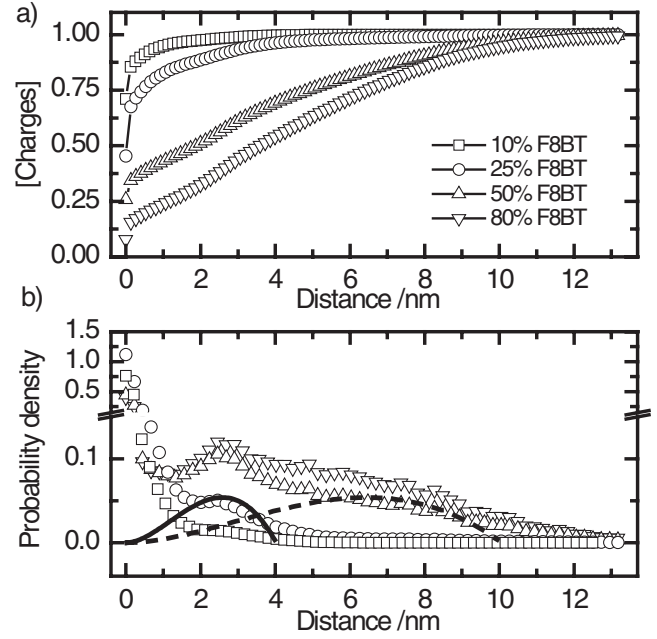


FIG. 3. Panels (a) and (b) are the cumulative distribution and probability density of the rms exciton diffusion length for PFB:F8BT blends, respectively. The dashed and solid lines show the theoretical distribution of exciton diffusion length for a sphere with  $R = 5 \text{ nm}$  and  $R = 2 \text{ nm}$ , respectively.

The data in Fig. 3(b) furthermore reveal that the experimental probability densities increase for all blend ratios, when the rms diffusion length becomes 0. The modeled curves approach 0 and this limiting behavior should be independent of domain size and shape. Thus, at early times our exciton energy transfer model underestimates the exciton transfer rates. We investigate this issue in the time domain and numerically solve the Fokker-Planck equation for exciton diffusion in spherical symmetry

$$\frac{\partial [Ex]}{\partial t} = H(r - R + a) D_1 \frac{1}{r^2} \frac{\partial (r^2 [Ex](r, t))}{\partial r} + D_2(t) \frac{1}{r^2} \frac{\partial}{\partial r} \left( \frac{r^2 \partial [Ex](r, t)}{\partial r} \right) - \frac{1}{\bar{\tau}_N(t)} [Ex], \quad (2)$$

with  $D_1$  as a drift constant, and  $D_2(t)$  as the time-dependent diffusion coefficient calculated as  $D_2(t) = R_{\max}/6t$  [see Fig. 2] [19], and  $\bar{\tau}_N(t)$  as the time-dependent average lifetime [20], calculated as  $\bar{\tau}_N(t) = \sum_i A_{N,i} \exp(-k_{N,i}t) / \sum_i A_{N,i} k_{N,i} \exp(-k_{N,i}t)$ .  $H$  is the Heaviside step function and depends on the radius of the domain  $R$  and the size of an interface region  $a$ . Equation (2) is constructed so that excitons undergo diffusion inside the domain and an additional drift component towards the heterojunction is active in the interface region (see inset of Fig. 4). The boundary conditions are  $[Ex](r = R) = 0$ , which imposes fast charge generation at the domain boundary, and  $\partial [Ex](r = 0) / \partial r = 0$ , which is required by the spherical symmetry.

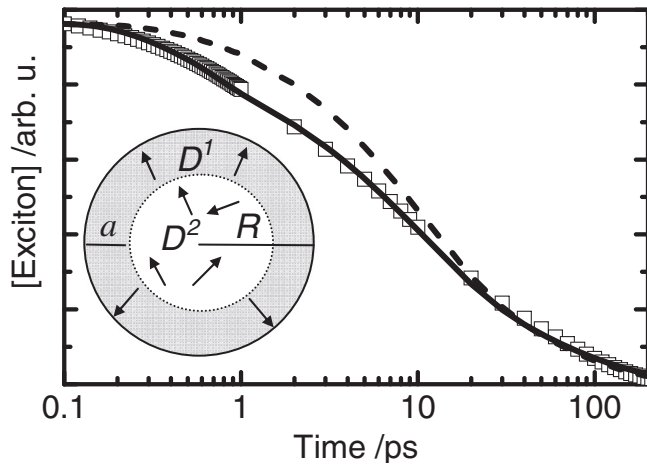


FIG. 4. Experimental (symbols) and modeled (lines) diffusion limited exciton decays are compared. The experimental data are the exciton decay ( $E_x$ ) reconstructed from the numerical fit presented in Fig. 1(c). Here we consider the exponential terms  $2 \leq j \leq 4$  in  $E_{CT}(t)$ , which ensures that only excitons that are generated in the bulk are treated. The modeled data are a fit using Eq. (2), with (dashed line) and without (solid line) the drift component close to the interface (see text). The inset shows a cartoon of the diffusion ( $D_2$ ) in the bulk of the domain and the additional drift towards the heterojunction ( $D_1$ ) in the interface region.

The symbols in Fig. 4 show the exciton decay due to natural recombination and quenching at the heterojunction for a F8BT:PFB blend with 50% F8BT content. We have solved Eq. (2) numerically for the range  $a = 0$  to  $a = 1.7$  nm,  $D_1 = 0$  to  $D_1 = -2$  nm/ps, and  $R = 2$  nm to  $R = 10$  nm and determine the best fit from the minimum SSR. When the drift is switched off (i.e.,  $a$  set to 0) the initial fast exciton decay is not reproduced by the model (dashed line). The best fit is for  $R = 3.6 \pm 0.12$  nm [18], which also underestimates the domain size as determined in Fig. 3(b). Solving Eq. (2) with the drift component at the interface region shows significantly better agreement with the experimental data (solid line). The best fit is for  $a = 0.78 \pm 0.17$  nm,  $D_1 = -0.9 \pm 0.4$  nm/ps, and  $R = 4.75 \pm 0.25$  nm [18], with the latter parameter now in agreement with the domain size as determined in Fig. 3(b). The existence of a drift component close to the heterojunction is consistent with excitons funneled efficiently to a potential energy minimum at the interface. Recently, it was predicted that the ground state potential energy is significantly reduced for certain chain segments at the phase boundary [17]. This is due to attractive Coulombic interaction with chromophores across the heterojunction. These sites also facilitate efficient exciton ionization [21]. Our finding here suggests that excitons transfer preferentially to these low-energy polymer seg-

ments, which is consistent with the high efficiency of exciton ionization observed in many binary blends for solar cell applications.

Finally, we note that by solving the diffusion equation [Eq. (2)] only the *average* domain size may be determined. It testifies to the strength of the previous approach leading to Fig. 3(b) that the *distribution* of phase sizes is resolved. This confirms that exciton diffusion is a powerful probe of nanoscale morphology that cannot be assessed by other techniques.

The authors acknowledge financial support from EPSRC and W.J.D. Beenken for discussions, S.W. thanks the Fitzwilliam College Cambridge for financial support, and I. A. H. thanks the Cambridge Commonwealth Trust for financial support.

\*Corresponding author.

sebastian.westenhoff@chem.gu.se

†Present address: Biochemistry & Biophysics, Department of Chemistry, Göteborg University, Box 462, SE-40530 Göteborg, Sweden.

- [1] J. J. M. Halls *et al.*, Nature (London) **376**, 498 (1995).
- [2] G. Yu *et al.*, Science **270**, 1789 (1995).
- [3] V. D. Mihailetschi *et al.*, Phys. Rev. Lett. **93**, 216601 (2004).
- [4] C. J. Brabec, N. S. Sariciftci, and J. C. Hummelen, Adv. Funct. Mater. **11**, 15 (2001).
- [5] P. Peumans, A. Yakimov, and S. R. Forrest, J. Appl. Phys. **93**, 3693 (2003).
- [6] A. C. Morteani *et al.*, Phys. Rev. Lett. **92**, 247402 (2004).
- [7] C. R. McNeill *et al.*, Nano Lett. **6**, 1202 (2006).
- [8] E. Hennebicq *et al.*, J. Am. Chem. Soc. **127**, 4744 (2005).
- [9] S. Westenhoff *et al.*, Phys. Rev. Lett. **97**, 166804 (2006).
- [10] S. C. J. Meskers *et al.*, J. Phys. Chem. B **105**, 9139 (2001).
- [11] R. Kersting *et al.*, Phys. Rev. Lett. **70**, 3820 (1993).
- [12] C. R. McNeill *et al.*, J. Phys. Chem. C **111**, 19 153 (2007).
- [13] M. A. Stevens *et al.*, Phys. Rev. B **63**, 165213 (2001).
- [14] N. Takeda, S. Asaoka, and J. R. Miller, J. Am. Chem. Soc. **128**, 16 073 (2006).
- [15] S. De *et al.*, J. Am. Chem. Soc. **129**, 8466 (2007).
- [16] See EPAPS Document No. E-PRLTAO-101-075827 for supplementary information. For more information on EPAPS, see <http://www.aip.org/pubservs/epaps.html>.
- [17] P. Sreearunothai *et al.*, Phys. Rev. Lett. **96**, 117403 (2006).
- [18] The fitting errors were determined as  $SSR(p) < SSR^*(1 - F[1, N - P]/(N - P))$ , with  $N$  and  $P$  as the number of parameters and data points, respectively,  $F$  as the  $F$  distribution for 99.99% confidence, and  $SSR(p)$  as the SSR minimized over all parameters except for  $p$ .
- [19] C. Daniel *et al.*, J. Phys. Chem. C **111**, 19 111 (2007).
- [20] D. E. Markov *et al.*, Phys. Rev. B **72**, 045216 (2005).
- [21] Y.-S. Huang *et al.*, Nat. Mater. **7**, 483 (2008).
- [22] G. D. Scholes and G. Rumbles, Nat. Mater. **5**, 683 (2006).